Self-assembled fluorescent magnetic nanoprobes for multimode-biomedical Imaging

Eun-Kyung Lim and Seungjoo Haam*
Department of Chemical and Biomolecular Engineering, College of Engineering, Yonsei University, Seoul 120-749, Republic of Korea
, ekekek@yonsei.ac.kr, haam@yonsei.ac.kr

ABSTRACT

We fabricated multimode nanoprobes for acquisition of biological information at different object levels, i.e., in vivo detection and ex vivo validation for characterizing tumor angiogenesis. Fluorescent magnetic nanoprobes (FMNPs) were synthesized by using amphiphilic pyrenyl polyethylene glycol (Py-PEG) and superparamagnetic MnFe2O4 nanocrystals (MNCs). Py-PEG, which is synthesized by conjugation of hydrophilic PEG with hydrophobic and fluorescent 1-pyrenebutyric acid through an esterification process, is capable of self-assemblyandmaintaining a highUVfluorescent intensity in aqueous phase. Py-PEG can be used as a fluorescent surfactant that simultaneously and efficiently encapsulates MNCs to exhibit fluorescent andmagnetic properties as well as maintaining highwater-solubility. Consequently,weproved that our biologically non-toxic FMNPs were prominent multimode imaging probes by showing not only excellent MR sensitivity but also high illumination intensity with strong signal strength under short exposure time of UV light from the extensive imaging studies of in vitro/vivo and ex vivo using orthotopic and xenograft mice models.

Keywords: Nanoprobe, Magnetic resonance imaging, Multimode, Fluorescent

1 INTRODUCTION

Molecular nanoprobes using well-tailored superparamagnetic nanocrystals are of great interest for detecting various biological objects via magnetic resonance (MR) imaging due to their highsensitivity and specificity gifted from a nanoeffect [1-4]. Further, the superparamagnetic nanocrystals as an MR contrast agent are hybridized with organic/inorganic fluorescent materials to create a single nanoplatform ofmultimodal imaging nanoprobes, which are utilized to measure in vivo biological events via MR and optical imaging at the same level of biological objects. In particular, both fluorescent and magnetic properties from conjugated multimodal imaging nanoprobes have been majorly used to render accurate appreciation of clinically significant events of cells, tissues and organisms via dual monitoring. Furthermore, a challenge for acquisition of biological information at different object levels, such as in vivo detection and ex vivo validation by using multimodal imaging methods to characterize tumor angiogenesis has been emerged [5-15]. Ultraviolet (UV) imaging has been recently introduced to provide higher spatial resolution with detailed insight into cellular events compared to visible light due to their shorter wavelength illumination. Thus, it would be of great significance to integrate MR imaging (in vivo) with UV imaging (ex vivo) for more robust acquisitionof biological event with higher spatial resolution.However forUV imaging, to acquire high spatial intra-cellular resolution while keeping the cells alive and undamaged as long as possible, higher illumination intensities and longer exposure times over which cells are observed before they exhibit signs of damage should be necessary to provide sufficient signal strength [16-18]. Herein, we presented a fluorescent magnetic nanoprobe (FMNP) as a multimodal imaging agent. The fabrication of FMNP began with synthesizing pyrenyl polyethylene glycol (Py-PEG) with methoxy poly(ethylene glycol) (PEG) and 1-pyrenebutyric acid (Py) exhibiting amphiphilic and UV fluorescent properties. Then a simultaneous self-assembly of hydrophobicmagnetic nanocrystals and Py-PEG as a fluorescent surfactant formed FMNPs utilized for UV and MR imaging capability (Figure. 1).

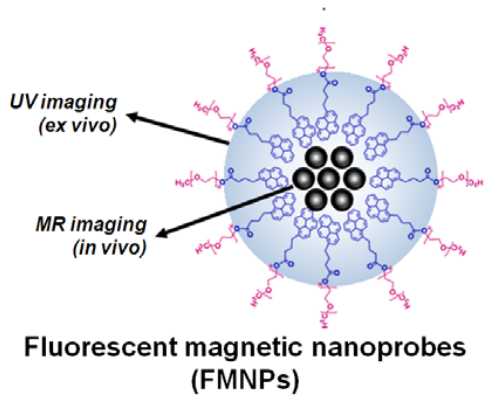

Figure 1: Schematic illustration of simultaneously self-assembled fluorescent magnetic nanoprobes (FMNPs) as multimodal biomedical imaging probes..

2 RESULT AND DISCUSSION

Monodispersed $MnFe_2O_4$ nanocrystals (MNCs) were synthesized as MR contrast agents by the thermal decomposition method. For phase transference of MNCs into aqueous phase and implementation of their fluorescent property at once, we synthesized a pyrenyl polyethylene glycol (Py-PEG) as a fluorescent surfactant by coupling of 1-pyrenebutyric acid and PEG by an esterification process. DCC was used to prepare active carboxylate from 1-pyrenebutyric acid. Then, the prepared carboxylate was coupled with DMAP as the nucleophilic catalyst through the labile ion pair between the carboxylate and the acetylpyridinium ions. Finally, the hydroxyl group of PEG, serving as a nucleophile, attacked the low electric carbon of the acetyl group to form an ester bond, and a protonated catalyst was reformed. Thus, the generated ester group of Py-PEG was confirmed at 1737 cm^{-1} and the hydroxyl group of PEG and carboxyl group of 1-pyrenebutyric acid were no longer observed at 3500 cm^{-1} and 1695 cm^{-1}, respectively. Moreover, successful synthesis of Py-PEG was further verified by its ^{1}H-NMR spectrum at 7.82 and 8.12 (-CHe from 1-pyrenebutyric acid) and 3.65 ppm (eCH2e in the PEG chain). In addition, the incremental change in molecular weight of Py-PEG from 5000 Da (naked PEG) to 5288 Da was evaluated by gel permeation chromatography analysis. Naked pyrene is insoluble inwater due to the non-polar and hydrophobic properties of its four symmetric fused benzene rings. However, PEGylated pyrene (Py-PEG) can be highly soluble inwater because of its hydrophilic property resulting fromhydrogen bonding between the oxygen atomsofPEGandwater molecules [19]. Due to the amphiphilic property of Py-PEG, the hydrophobic pyrenyl group of Py-PEG is surrounded by hydrophilic PEG chains. As the Py-PEG concentration increased, the fluorescence intensity ratio of Py-PEG (I_{396}/I_{376}) spontaneously declined and the critical micelle concentration was 40.6 nm . In addition, the pyrene molecules of Py-PEG maintained a high electron density compared to the naked pyrene molecules and exhibited strong excited-state dimers (excimer) because of the closely packed pyrene units in the Py-PEG micelle. The synthesized Py-PEG exhibited a high fluorescent intensity at 375 and 398 nm and strong excimer at 420 nm due to interactions between the excited pyrene molecules of Py-PEG and another pyrene molecule in the ground electronic state, promoted by the high electron density of pyrene molecules.29 These results indicate that the synthesized Py-PEG successfully played a role of amphiphilic fluorescent surfactant forfabrication of FMNPs. To synthesize water-soluble FMNPs, hydrophobic MNCs were encapsulated by the amphiphilic fluorescent surfactant, Py-PEG, using a nano-emulsion method.MNCs in organic solvent were simultaneously wrapped by the self-assembly of Py-PEG molecules and water-soluble FMNPs were subsequently formulated by evaporation of the organic phase during the nanoemulsion process. Transmission electron microscopy (TEM) and laser scattering analysis indicated complete dispersion of FMNPs in water with a consistent size distribution (64.1 ± 3.1 nm), whichwas similar to the observed dispersion of FMNPs in biological medium (10% fetal bovine serum and 1% penicillin streptomycin in DMEM) (69.8 ± 2.1 nm). FMNPs enveloped by non-ionic PEG molecules exhibited - 0.4 ± 0.6 mV in water and -1.5 ± 0.3 mV in biological medium. In addition, FMNPs (533.5 ×10-2 mg/mL) were stable in a wide range of salt solutions (up to 1 M) and pH conditions (pH 4 - 9) without any aggregations. While thermogravity analysis demonstrated that the organic compounds in FMNPs were 50 wt%, the mixed spinel structure of theMNCswas still maintained (2θ: 30.3° (220), 35.8° (311), 43.6° (400), 53.7° (422), 57.5° (511), and 62.7° (440)). Furthermore, FMNPs exhibited superparamagnetic behavior at 298 K without remanence and coercivity and the saturation of magnetization at 0.8 T of FMNPswas 41.9 emu/g ofMNCs, whichwas similar to that for naked MNCs (43.2 emu/g of MNCs). To evaluate the potential use of FMNPs as ultrasensitive MR imaging contrast agents, we investigated MR images of the FMNP solution and the signal intensities. T2-weighted MR images exhibited strong black color for the thicker FMNP solution and the corresponding relaxivity coefficient of FMNPs containing MNCs was 786.4$mM^{-1}s^{-1}$ indicating that the FMNP solution has sufficient high-sensitivity for use as an MR imaging contrast agent. To confirm the utility of FMNPs as optical imaging agents, we also investigated the fluorescence properties of FMNPs (λex: 345 nm and λem: 397 nm). The fluorescence spectra of FMNPs are similar to those of Py-PEG, and even after loading MNCs into FMNPs the fluorescent peak from excimer at 420 nmwas maintained. Furthermore, water-soluble FMNPs exhibit vivid luminescent light under UVlamp (λ_{ex}: 365 nm) and FMNPs are magnetically gathered by an external magnetic field (Nd-B-Fe magnet, 0.3 T), maintaining the fluorescent properties of the pyrene n the FMNPs. These excellent magnetic and optical properties of FMNPs provide abundant possibilities for multimodal-biomedical imaging. To examine the cellular cytotoxicity of FMNPs, an MTT assay was performed using NIH3T6.7 cells treated with FMNPs. FMNPs exhibited biocompatibility without any inhibitory effect on growth and proliferation in the target NIH3T6.7 cells, even at a high concentration of 1.6 mg/mL. For assessment of the optical imaging performance of FMNPs, NIH3T6.7 cells were incubated with the non-cytotoxic FMNPs (21.3 mg/mL) and then visualized under UV light. The fluorescent microscopic images of NIH3T6.7 cells treated with FMNPs revealed vivid fluorescent blue light in the cytosol due to fluid endocytosis of FMNPs, whereas there was no fluorescent blue staining in untreated cells (control).9 The red fluorescence represents nuclear site staining by Lyso tracker (10 nm). Due to the presence of pyrene from FMNPs, NIH3T6.7 cells treated with FMNPs also demonstrated a distinct luminescent light under UV lamp (λex: 365 nm) compared with untreated control cells. The results from Prussian blue staining and TEM images are consistent with the optical imaging results. We next investigated the MR contrast effect of FMNPs in NIH3T6.7

cells monitored at 1.5 T. A significant MR contrast effect was observed in treated cells (black color) compared to non-treated control cells (bright gray color). The calculated R2 value of NIH3T6.7 cells treated with FMNPs was 14.5 s^{-1}, which was 387.6 % ($\triangle$ $R2/R2_{Non\text{-}treatment}$) higher than that of non-treated cells (2.9 s^{-1}). Prussian blue and ferric ions of the MNCs in FMNPs rapidly exchange electrons thereby producing dark blue colors in the intra-cellular region. In the TEM images, the black clusters of NIH3T6.7 cells treated with FMNPs indicate the engulfment of FMNPs into the intra-cellular region. The concentration of MNCs (Mn and Fe ions) in NIH3T6.7 cells treated with FMNPs was 9.1 mg/mL (3.0×10^5 cells) measured by inductively coupled plasma mass spectrometry (ICP-MS) analysis. Furthermore, the well-dispersed NIH3T6.7 cells treated with FMNPs were sensitively and rapidly moved toward a permanent magnet exhibiting an intense luminescence under an external magnetic field (NdeBeFe magnet, 0.3 T). These results demonstrate that FMNPs are suitable for use as molecular nanoprobes for highly versatile imaging and ultrasensitive detection at the cellular level. We next performed MR imaging of xenograft mice models using FMNPs as an MR contrast agent for passive cancer detection. First, nude mice were subcutaneously implanted in the proximal thigh with NIH3T6.7 cells to develop xenograft mouse model. Magnetic resonance (MR) images were then obtained before and after intravenous injection of FMNPs (300 μ g Fe + Mn in FMNPs), respectively. After the injection of FMNPs (post-injection), the T2 value was immediately dropped at tumor site (increase in $\triangle R2/$ R2Pre value; $\triangle R2 = R2 - R2_{Pre}$) and strong MR signal intensity was observed compared to pre-contrast images. In T2-weighted MR images, the black color gradually spread out along change of the T2 value ($R2 = 1/T2$; $\triangle R2/ R2_{Pre}$: 64.16%), following the peripheral blood vessel of tumor area because the FMNPs were diffused and permeated to tumor tissues across corresponding vascular distributions due to enhanced permeation and retention (EPR) effect.[2,20] Furthermore, we performed ex vivo MR imaging of tumor tissue which explanted from a xenograft model treated with FMNPs, presented partially black color compared with non-treated tumor tissue. The MR image of tumor tissue exhibited the existence of fairly high amount of FMNPs ($\triangle R2/R2_{Non\text{-}treatment}$: 90.27%) due to blood pool effect and/or EPR effect of the tumor site. These results indicate promising potential application of FMNPs to detect the tumor as MR contrast agent. On the other hand, we next determined whether FMNPs are capable of detecting intratumoral tissue architecture which requires high resolution of cellular level via fluorescent microscopy at UV spectral bands.We analyzed the frozen ex vivo samples of tumor and muscle by using fluorescence microscopy. We observed vivid fluorescent blue and dark blue color dots in the interior of tumor tissue treated FMNPs, also confirmed MNCs of FMNPs were co-existence with fluorescenct properties through the Prussian blue staining images. These results indicated that blue dots in ex vivo tumor tissue successfully confirmed the presence of FMNPs at microscopic resolution which was shown at in vivo MR images. In addition, we verified the passive tumor tissue detection capability of FMNPs as universal bimodal imaging nanoprobes by using blood pooling and/ or EPR effect. Orthotopic bladder cancer mouse model was used in this experiment because it is more physiologically mimicking human cancer compared to xenograft one in terms of tumor neoangiogenesis based on "seed and soil" theory.[21-23] Interestingly, we observed an immediate decrease of the T2 value ($\triangle R2/R2_{Pre}$: 42.93%), following the central blood vessel of tumor site after FMNPs were spread out and permeated to tumor tissues by EPR effect.[20] In addition, ex vivo MR imaging of tumor tissue from orthotopic model treated with FMNPs cross checked the evidence of existence of FMNPs in comparison to the untreated model as well ($\triangle R2/R2_{Non\text{-}treatment}$: 44.91%). These findings indicated that FMNPs demonstrated similar high performance imaging capability in orthotopic mouse model as well as xenograft mouse model.

3 CONCLUSION

We introduce a facile and efficient strategy to fabricate FMNPs for universal nanoprobes to cover ex vivo high resolution modality at the cellular level as well as that of in vivo MRI. Py-PEG can be used as a fluorescent surfactant that simultaneously and efficiently encapsulates MNCs to induce fluorescent and magnetic properties as well as water-solubility. From the complete in vitro/vivo studies as well as ex vivo ones by using both orthotopic and xenograft mice models, FMNPs showed not only excellent sensitivity and feasibility as MR probes but also high illumination intensities and strong signal strength for short exposure times as UV imaging probes as well as exhibiting sufficient biocompatibility. Apart from the currently developed multimodal nanoprobes, it may be interesting to speculate the undiscovered merits of UV fluorescence/MRI multimode nanoprobes for better spatial resolution to obtain detailed biological information. Moreover, since a variety of hydrophobic fluorescent dyes and drugs can be easily assembled with hydrophobic core, this study may be extended to synthesize versatile nanocomplexes for imaging probes, drug delivery and cell separation.

REFERENCES

[1] Weissleder R, Pittet MJ. Imaging in the era of molecular oncology. Nature 2008;452:580-9.

[2] Lee J-H, Huh Y-M, Jun Y-W, Seo J-W, Jang J-T, Song H-T, et al. Artificially engineered magnetic nanoparticles for ultra-sensitive molecular imaging. Nat Med 2007;13:95-9.

[3] Huh Y-M, Jun Y-W, Song H-T, Kim S, Choi J-S, Lee J-H, et al. In vivo magnetic resonance detection of cancer

by using multifunctional magnetic nanocrystals. J Am Chem Soc 2005;127:12387-91.
[4] Jun Y-W, Huh Y-M, Choi J-S, Lee J-H, Song H-T, Cheon J, et al. Nanoscale size effect of magnetic nanocrystals and their utilization for cancer diagnosis via magnetic resonance imaging. J Am Chem Soc 2005;127:5732-3.
[5] Bertorelle F, Wilhelm C, Roger J, Gazeau F, Manager C, Cabuil V. Fluorescencemodified superparamagnetic nanoparticles: intracellular uptake and use in cellular imaging. Langmuir 2006;22:5385-91.
[6] Lee J-H, Jun Y-W, Yeon S-I, Shin J-S, Cheon J. Dual-mode nanoparticle probes for high-performance magnetic resonance and fluorescence imaging of neuroblastoma. Angew Chem Int Ed 2006;45:8160-2.
[7] Tsai C-P, Hung Y, Chou Y-H, Huang D-M, Hsiao J-K, Chang C, et al. Highcontrast paramagnetic fluorescent mesoporous silica nanorods as a multifunctional cell-imaging probe. Small 2008;4:186-91.
[8] Yang J, Lee J, Kang J, Chung C-H, Lee K, Suh J-S, et al. Magnetic sensitivity enhanced novel fluorescent magnetic silica nanoparticles for biomedical applications. Nanotechnology 2008;19:075610-5.
[9] Yang J, Lim E-K, Lee HJ, Park J, Lee SC, Lee K, et al. Fluorescent magnetic nanohybrids as multimodal imaging agents for human epithelial cancer detection. Biomaterials 2008;29:2548-55.
[10] Seo S-B, Yang J, Lee E-S, Jung Y, Kim K, Lee S-Y, et al. Nanohybrids via a polycation-based nanoemulsion method for dual-mode detection of human mesenchymal stem cells. J Mater Chem 2008;18:4353-484.
[11] Kim J, Lee JE, Lee J, Yu JH, Kim BC, An K, et al. Magnetic fluorescent delivery vehicle using uniform mesoporous silica spheres embedded with monodisperse magnetic and semiconductor nanocrystals. J Am Chem Soc 2005;128:688-9.
[12] Medarova Z, Pham W, Kim Y, Dai G, Moore A. In vivo imaging of tumor response to therapy using a dual-modality imaging strategy. Int J Cancer 2006;118:2796-802.
[13] Josephson L, Kircher MF, Mahmood U, Tang Y, Weissleder R. Near-infrared fluorescent nanoparticles as combined MR/optical imaging probes. Bioconjug Chem 2002;13:554-60.
[14] Vuu K, Xie J, McDonald MA, Bernardo M, Hunter F, Zhang Y, et al. Gadoliniumerhodamine nanoparticles for cell labeling and tracking via magnetic resonance and optical imaging. Bioconjug Chem 2005;16:995-9.
[15] Talanov VS, Regino CAS, Kobayashi H, Bernardo M, Choyke PL, Brechbiel MW. Dendrimer-based nanoprobe for dual modality magnetic resonance and fluorescence imaging. Nano Lett 2006;6:1459-63.
[16] Parpura V, Tong W, Yeung ES, Haydon PG. Laser-induced native fluorescence (LINF) imaging of serotonin depletion in depolarized neurons. J Neurosci Methods 1998;82:151-8.
[17] Lillard SJ, Yeung ES. Temporal and spatial monitoring of exocytosis with native fluorescence imaging microscopy. J Neurosci Meth 1997;75:103-9.
[18] Lillard SJ, Yeung ES, McCloskey MA. Monitoring exocytosis and release from individual mast cells by capillary electrophoresis with laser-induced native fluorescence detection. Anal Chem 1996;68:2897-904.
[19] Jeon SI, Lee JH, Andrade JD, De Gennes PG. Proteinesurface interactions in the presence of polyethylene oxide: I. Simplified theory. J Colloid Interface Sci 1991;142:149-58.
[20] Yang J, Lee T-I, Lee J, Lim E-K, Hyung W, Lee C-H, et al. Synthesis of ultrasensitive magnetic resonance contrast agents for cancer imaging using PEGfatty acid. Chem Mater 2007;19:3870-6.
[21] Tanaka T, Shiramoto S, Miyashita M, Fujishima Y, Kaneo Y. Tumor targeting based on the effect of enhanced permeability and retention (EPR) and the mechanism of receptor-mediated endocytosis (RME). Int J Pharmaceut 2004;277:39-61.
[22] Debatin JGF, Nadel SN, Paolini JF, SostmanHD, ColemanRE, Evans AJ, et al. Cardiac ejectionfraction: phantom study comparing cine MRimaging, radionuclideblood pool imaging, and ventriculography. J Magn Reson Imaging 1992;2:135-42.
[23] Son YJ, Jang J-S, Cho YW, Chung H, Park R-W, Kwon IC, et al. Biodistribution and anti-tumor efficacy of doxorubicin loaded glycol-chitosan nanoaggregates by EPR effect. J Control Release 2003;91(1-2):135-45.

[1] Nanotech 2010, 696 San Ramon Valley Boulevard, Suite 423, Danville, CA 94526-4022, Ph: (925) 353-5004, Fax: (925) 886-8461, swenning@nsti.org.